A Multiaxial Constitutive Model for Fibre-reinforced Sand

Zhiwei Gao*[1], Andrea Diambra[$]

*James Watt School of Engineering, University of Glasgow, Glasgow, G12 8QQ, UK
[$]CAME School of Engineering, University of Bristol, Bristol, BS8 1QU, UK
[1]Corresponding author. Email: Zhiwei.gao@glasgow.ac.uk.

ABSTRACT: Fibre orientation in fibre-reinforced sand (FRS) is highly anisotropic due to compaction during sample preparation or field construction. This makes the mechanical behaviour of FRS, such as strength and dilatancy, highly dependent on the strain increment direction. While constitutive models able to capture such anisotropic behaviour of FRS have been proposed for conventional triaxial compression and extension conditions only, this paper proposes for the first time a full anisotropic model for FRS formulated in the general multiaxial stress space. The new model is developed based on the assumption that the strain of FRS is dependent on the deformation of the sand skeleton. In turn, the fibre presence affects the void ratio and effective stress of the soil skeleton, which governs the elastic properties, dilatancy and plastic hardening of the FRS. The effect of anisotropic fibre orientation on the FRS behaviour is considered through an anisotropic variable which characterises the relative orientation between the loading direction tensor and fibre orientation tensor. The model does not require direct measurement of the stress-strain relationship of individual fibres. Though the model is for FRS under multiaxial loading conditions, the parameters associated with the fibre inclusion can be determined based on triaxial test results, provided that the orientation of fibres is known. The model has been used to predict the stress-strain relationship of fibre-reinforced Hostun RF (S28) sand under multiaxial loading conditions. Satisfactory agreement between the experimental data and model predictions is observed.

Keywords: Fiber-reinforced sand, multiaxial model, critical state, dilatancy, anisotropy

1. INTRODUCTION

Soil improvement is widely used in geotechnical engineering to enhance the strength and stiffness of soils for construction of infrastructure such as buildings, road embankments, airfields and slopes. In particular, soil reinforcement using flexible fibres is found to be a promising method for slope stabilization, as the fibres can both enhance the soil strength and resistance to crack development due to drying and wetting cycles (Gray & Ohashi, 1983; Sonnenberg et al., 2010; Silva Dos Santos et al., 2010; Santoni & Webster, 2001; Zornberg, 2002; Tang et al., 2012; Shukla, 2017). Some preliminary attempts of field applications have been reported in the literature (e.g. Santoni & Webster, 2001; Shukla, 2017), although more work is necessary to break the current technological barriers.

An important feature of fibre reinforced sands (FRS) is the anisotropic fibre orientation caused by compaction during sample preparation or field construction (Michalowski & Čermák, 2002; Diambra et al., 2007; Soriano et al., 2017). Such anisotropic fibre orientation makes the mechanical behaviour of FRS dependent on the strain increment direction (Michalowski & Čermák, 2002; Diambra et al., 2013; Gao & Zhao, 2013). For the same FRS with preferred fibre orientation being horizontal, fibres are found to add significant enhancement to the soil strength in conventional triaxial compression, where the direction of major principal stress/strain increment is vertical, and almost negligible reinforcement in conventional triaxial extension with horizontal major principal stress/strain increment direction (Michalowski & Čermák, 2002; Diambra et al., 2013; Mandolini et al., 2018). This is caused by the relative orientation of fibres with respect to the developed tensile strains within the soil (Diambra et al., 2007; Soriano et al., 2017): the fibres' strengthening contribution is activated only when they are pulled in tension. Thus, it appears paramount to account for the effect of fibre orientation anisotropy in modelling the mechanical behaviour of FRS (Michalowski & Čermák, 2002; Diambra et al., 2013; Mandolini et al., 2018).

Indeed, some attempts have been made in modelling the anisotropic response of FRS, most of which have focused on the yield or failure condition. For instance, an energy-based method for modelling the shear strength of FRS has been proposed by Michalowski and his co-workers, in which the anisotropic fibre orientation is accounted for (Michalowski & Zhao, 1996; Michalowski & Čermák; 2002). Gao & Zhao (2013) developed a failure criterion for FRS by using a fabric tensor which describes the anisotropic fibre orientation in FRS. The failure criterion has been verified by existing test data. However, only a few attempts have been made in modelling the complete stress-strain relationship and dilatancy response of FRS before failure, which is of importance for practical geotechnical design using this soil improvement technique.

The first constitutive model for FRS was proposed by di Prisco & Nova (1993). This model gives reasonable prediction of soil failure but, due to the simple model adopted for the sand matrix, is unable to simulate dilatancy and post-peak softening. Ding & Hargrove (2006) have proposed a model for characterizing the nonlinear elastic stress-strain relationship of FRS. Diambra et al. (2010) and Diambra et al. (2013) were the first to develop an anisotropic constitutive model for FRS which can satisfactorily describe the stress-strain relationship in both triaxial compression and extension. The model framework was also applied to fibre reinforced clays (Diambra and Ibraim, 2014). An important feature of the model is that the stress tensor characterizing the fibre-reinforcement effect needs to be obtained through an integration which is dependent on the induced domain of tensile strains and fibre orientation. This integration can be readily done for axisymmetric loading conditions like triaxial compression/extension, where the areas of compression and extension can be easily defined, but considerably difficulties arise for more complex and general multiaxial stress paths. Therefore, the model has yet to be extended to the generalized multiaxial stress space (Diambra et al., 2013). There is indeed no existing constitutive model which is suitable for describing the mechanical response of FRS under multiaxial loading conditions.

A new constitutive model for FRS developed in the generalised multiaxial stress space is presented in this study. The proposed modelling framework treats the fibre reinforced soil as a unique composite material and builds on the well-established constitutive modelling framework by Li & Dafalias (2002). While the yield locus for the fibre reinforced is expressed in terms of the overall composite stress, it is assumed that the main behavioural features (hardening rule, elastic properties and dilatancy) are governed by the sand matrix, whose density and stress states are affected by the presence and contribution of the fibres. The anisotropic stress contribution of the fibres is modelled through the introduction of an anisotropic variable A expressed in terms of a joint invariant of the loading direction tensor n_{ij} and a deviatoric fibre orientation tensor F_{ij}. Compared to the baseline sand constitutive model by Li & Dafalias (2002), four additional parameters are introduced to characterize the effect of fibre inclusion on mechanical response of FRS. While model capabilities are challenged and validated against multiaxial experimental tests, it will be shown that all the fibre parameters can be readily determined using triaxial compression and extension test data.

2. NOTATION

While the model will be developed for a unique composite material, it is still necessary to define stress and strain quantities for the FRS, the sand skeleton and the fibres phase. The stress and strain states of the composite are defined by tensor σ_{ij} and ε_{ij}, respectively. The isotropic stress component is defined by $p = \sigma_{ii}/3$, while $s_{ij} = \sigma_{ij} - p\delta_{ij}$ is the deviatoric stress tensor with δ_{ij} being the Kronecker delta ($= 1$ for $i = j$, and $= 0$ for $i \neq j$). The deviator stress is defined as $q = \sqrt{\frac{3}{2} s_{ij} s_{ij}}$. Incremental volumetric strain is defined as $d\varepsilon_v = d\varepsilon_{ii}$, while deviatoric strain as $d\varepsilon_q = \sqrt{\frac{2}{3} de_{ij} de_{ij}}$, with the incremental deviatoric strain tensor defined as de_{ij} $(= d\varepsilon_{ij} - \frac{1}{3} d\varepsilon_v \delta_{ij})$.

3. FIBRE-SOIL INTERACTION MECHANISMS

3.1 Failure of fibre reinforced soils

Several studies have assumed that the shear strength of fibre reinforced material is the results of the contribution of the host soil and the fibre reinforcement (Michalowski & Čermák, 2002; Zornberg, 2002; Diambra et al., 2013; Gao & Zhao, 2013). Like the approach commonly used for cemented soils (Gao and Zhao, 2013; Festugato et al., 2018) have demonstrated that the failure criterion of FRS can be expressed as a modification of the strength criterion of granular soils as follows:

$$q = M_c g(\theta)(p + \bar{p}^f) \tag{1}$$

where M_c is the stress ratio q/p at failure for the unreinforced soil, $g(\theta)$ is an interpolation function to account for the strength dependency on the Lode angle θ, and $\bar{p}^f$ is the stress contribution of the fibres at failure. Eq. (1) assumes that, at the failure state, the sand skeleton 'feels' a mean effective stress $p + \bar{p}^f$ greater than the externally applied mean effective stress p, and in turn this triggers an increased shear strength for the FRS. Thus, one can use the following p^s and s_{ij}^s to describe the failure of FRS

$$p^s = p + \bar{p}^f \tag{2}$$

$$s_{ij}^s = s_{ij} \tag{3}$$

which renders $q^s = M_c g(\theta) p^s$ at failure. According to previous development of Gao and Zhao (2013) by analysing a large database of fibre reinforced sand strength, the maximum stress contribution of the fibre phase at failure can be expressed as:

$$\bar{p}^f = \chi p_a [1 - \exp(-\kappa p / p_a)] \tag{4}$$

where χ is a variable, dependent on both fibre content and fibre orientation, which governs the fibre contribution and which will be will be explained in more details in the subsequent section; p_a (=101 kPa) is the atmospheric pressure; κ is a parameter which account for the effect of stress level through the exponential term $\exp(-\kappa p / p_a)$ which models an improved fibre-soil interaction mechanism with increased stress level as discussed in Diambra and Ibraim (2015).

3.2 The fibre stress contribution and the effective sand skeleton stress tensor

Eqs. (2) and (3) can be expanded to pre-failure conditions to define a general expression for p^s and the effective sand skeleton stress tensor σ_{ij}^s, with s_{ij}^s being expressed as Eq. (3) above:

$$p^s = p + p^f \tag{5}$$

$$\sigma_{ij}^s = s_{ij}^s + p^s\delta_{ij} = s_{ij} + (p + p^f)\delta_{ij} \tag{6}$$

where p^f is a strain-level dependent variable characterizing the fibre-reinforcement effect. The fibre reinforcement stress p^f increases with the strain of FRS and finally reaches the maximum at the failure state when the fibres yield or pull out (Zornberg, 2002; Diambra et al., 2013; Gao & Zhao, 2013). Therefore, it can be assumed that the stress contribution of the fibres p^f varies from 0 at $\varepsilon_q = 0$ to $\bar{p}^f$ at sufficiently large ε_q. Evolution of p^f with shear strain ε_q can be defined in incremental terms using the following equation:

$$dp^f = \mu \frac{\bar{p}^f - p^f}{1+e} \sqrt{\frac{p}{p_a}}\, d\varepsilon_q \tag{7}$$

where μ is a model parameter governing the rate of fibre stress mobilisation for a given strain increment and it somehow accounts for the fibre stiffness and imperfect contact at the fibre-soil interface (see Diambra and Ibraim, 2015). Eq.(7) also models an improved fibre stress efficiency (i.e larger mobilised stress for the same strain level) for higher soil densities and higher stress level through the terms $\frac{1}{1+e}$ and $\sqrt{\frac{p}{p_a}}$ respectively, as experimentally evidenced by Diambra et al. (2010) among others. It should be noted that fibres may mobilise some stress also in pure isotropic compression conditions (e.g. Consoli et al. 2005) or they may still be stretched when $d\varepsilon_v < 0$ (volume expansion) with $d\varepsilon_q = 0$, thus p^f should also changes with the volumetric deformation, ε_v, of the FRS. However, this appears to be a secondary contribution during shearing, and it is neglected for the sake of simplicity and to avoid the introduction of further model parameters.

3.3 Anisotropic fibre stress contribution

3.3.1 Fibre orientation tensor H_{ij}

It is found that the fibre-reinforcement to sand strength is the most significant in conventional triaxial compression (CTC) where the direction of the major principal stress σ_1 (also the direction of major principal strain increment $d\varepsilon_1$) is perpendicular to the preferred fibre orientation plane, induced by conventional sample preparation techniques (Michalowski, 2008; Diambra et al., 2013; Gao and Zhao, 2013; Mandolini et al., 2018). In conventional triaxial extension (CTE), where σ_1 is parallel to the preferred fibre orientation plane, very little or no fibre-reinforcement to soil strength is observed (Diambra et al., 2013; Mandolini et al., 2018). Therefore, χ $(or\ \bar{p}^f)$ should be the maximum in CTC and minimum (or even negligible) in CTE. Before specifying the variation of χ with the strain increment direction (or major principal stress direction) due to fibre orientation anisotropy, a tensor for describing the fibre orientation in FRS needs to be introduced.

As shown in Gao & Zhao (2013), a second-order tensor H_{ij} can be used for describing the fibre orientation in FRS:

$$H_{ij} = \oiiint \rho(\boldsymbol{n})\, n_i n_j dV \qquad (8)$$

where V is the total volume of a representative volume element of FRS (Fig. 1); n_i is the i-th component of the unit vector aligning in direction $\boldsymbol{n}$; $\rho(\boldsymbol{n})$ is the fiber concentration (ratio of the volume of fibres and sand particles) in direction $\boldsymbol{n}$. This definition of H_{ij} is similar to the fabric tensors used in some previous research on constitutive modelling of sand (Li and Dafalias, 2002; Taiebat and Dafalias, 2008; Li and Dafalias, 2012; Loukidis and Salgado, 2011; Woo and Salgado, 2015). In theory, a REV is the smallest volume on which measurement on stress and strain can be made that will yield values representative of the whole FRS. It must include enough sand particles and fibres. When the fibre orientation is measured for getting the fibre concentration function $\rho(\boldsymbol{n})$, a proper REV should be chosen. For simplicity, the entire soil sample is typically used (e.g., Diambra et al. 2007), which is bigger than a REV. But the result will not be affected when the sample used is larger than a REV.

For cross-anisotropic fibre orientation, we can further employ a simplified fiber distribution function $\rho(\beta)$ (Michalowski & Čermák, 2002; Diambra et al., 2007; Soriano et al., 2017) to characterize the fibre concentration, where β is the vertical angle of fibre inclination to the preferred fibre orientation plane (e.g., $x-y$ plane in Fig. 1). Both $\rho(\beta)$ and $\rho(\boldsymbol{n})$ must satisfy the following requirement (Michalowski & Čermák, 2002)

$$\frac{1}{V}\oiiint \rho(\boldsymbol{n})\, dV = \frac{1}{V}\oiiint \rho(\beta) dV = \rho_f \tag{9}$$

where ρ_f $(= v_f/v_s)$ is the average fibre concentration, with v_f and v_s being the volume of fibres and dry sand, respectively. ρ_f can be also expressed in terms of the fibre weight content w_f (ratio of fibre and dry sand weight), which is more frequently used in existing literature, as below

$$\rho_f = \frac{v_f}{v_s} = \frac{w_f G_s v_s / G_f}{v_s} = \frac{w_f G_s}{G_f} \tag{10}$$

where G_s and G_f denote the specific gravities of sand and fibres, respectively.

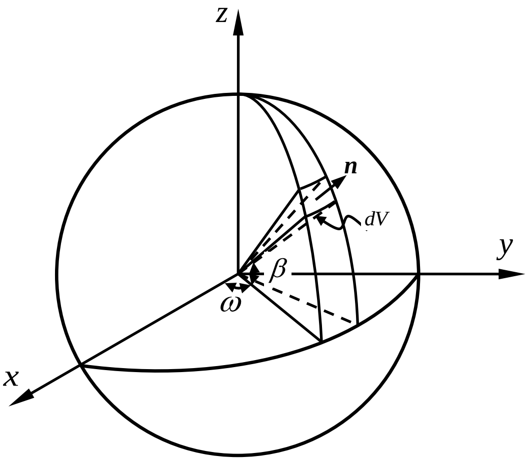

Fig. 1 A spherical representative volume element for fiber-reinforced soils (after Michalowski and Čermák, 2002)

According to Diambra et al. (2007) and Mandolini et al. (2018), $\rho(\beta)$ can be defined as below for FRS prepared in laboratories

$$\rho(\beta) = \rho_0 + \rho_a \cos^k \beta \tag{11}$$

where ρ_0, ρ_a and k are fitting parameters which can be determined based on the measured fibre orientation in FRS. It is shown by Diambra et al. (2007) and Soriano et al. (2017) that $\rho(\beta)$ expressed in Eq. (11) can give satisfactory description of cross-anisotropic fibre orientation in an FRS sample.

The fibre orientation tensor H_{ij} defined in Eq. (8) can always be decomposed into an isotropic part and deviatoric part F_{ij}:

$$H_{ij} = \frac{1}{3}\rho_f\left(\delta_{ij} + F_{ij}\right) \tag{12}$$

The deviatoric part of the fibre orientation tensor F_{ij}, which characterizes the fibre orientation anisotropy, will be used in the model formulations. For a axisymmetric FRS sample prepared through vertical compaction, F_{ij} can be expressed as below (Gao & Zhao, 2013; Gao et al., 2014)

$$F_{ij} = \begin{bmatrix} F_z & 0 & 0 \\ 0 & F_x & 0 \\ 0 & 0 & F_y \end{bmatrix} = \sqrt{\frac{2}{3}}\begin{bmatrix} -F & 0 & 0 \\ 0 & F/2 & 0 \\ 0 & 0 & F/2 \end{bmatrix} \tag{13}$$

where F_z, F_x and F_y represent the components of F_{ij} in the vertical and horizontal directions as shown in Fig.1. F $(= \sqrt{F_{ij}F_{ij}})$ is referred to as the degree of fibre orientation anisotropy. $F = 0$ indicates isotropic fibre orientation and $F > 0$ means anisotropic fibre orientation. Note that if one chooses a different coordinate system, a corresponding orthogonal transformation must be carried out to get the components of F_{ij} (Li & Dafalias, 2002; Gao et al., 2010; Gao et al., 2014). Hand calculations or CT scan of fibre orientation in the FRS can be used to determine the parameters ρ_0, ρ_a and k, and the value of F (Diambra et al., 2007; Soriano et al., 2017)

3.3.2 Variation of fibre stress contribution with loading conditions

The anisotropy of the fibre stress contribution is modelled by assuming a dependency of the variable χ in $\bar{p}^f$ (Eq. 4) with the applied direction of loading. A general form of χ should consider the influence of various factors (Ranjan et al., 1996; Diambra et al., 2013), which are discussed in Appendix 1. In this study, focus is placed on the variation of fibre-reinforcement (through χ and in turn $\bar{p}^f$ as per Eq.(4)) for a given FRS (i.e. fixed fibre content ρ_f and fibre orientation anisotropy F) with loading condition. Specifically, the following simple equation is used for χ

$$\chi = \chi_r \phi(A) \tag{14}$$

with

$$\phi(A) = \frac{1}{2}(1 - A) \text{ with } A = F_{ij} n_{ij} / F \tag{15}$$

where χ_r is a model parameter and A is the anisotropic variable (Gao & Zhao, 2013; Gao et al., 2014) depending on the deviatoric part of the orientation tensor (F_{ij}) and on the loading direction tensor n_{ij} which represents the plastic deviatoric strain increment direction and which will be expressed later in section 4.1.).

The anisotropic variable A describes the relative orientation between the plastic strain increment direction and fibre orientation. Since the total strain increment is very close to the plastic strain increment for sand, the physical significance of $\phi(A)$ is that the fibre-reinforcement effect varies with the relative orientation between the total strain increment direction and fibre orientation, which has been observed in laboratory tests (Michalowski & Čermák, 2002; Michalowski, 2008; Mandolini et al., 2018). For an FRS sample with cross-anisotropic fibre orientation, large values of A (equal or close to 1) are associated with coaxial (or close to coaxial) F_{ij} and n_{ij} tensors, meaning more fibres are oriented in the direction of compressive strains. As such, large values of A results in low values of function $\phi(A)$, and in turn a low fibre-reinforcement contribution, through low values of χ and $\bar{p}^f$.

Fig. 2 shows the variation of A and $\phi(A)$ with the orientation of the major principal stress direction relative to the vertical axis α in a torsional shear tests (e.g. an hollow cylindrical sample as per the experimental results of Mandolini et al. (2018) which will be simulated later in this paper) where a constant intermediate principal stress ratio b ($b = (\sigma_2 - \sigma_3)/(\sigma_1 - \sigma_3)$), where σ_2 is the intermediate principal stress and σ_3 is the minor principal stress) is maintained. The fabric tensor in Eq. (13) is used in the calculation and vertical axisymmetry of the fibre orientation distribution is assumed (Michalowski & Čermák, 2002, Diambra et al., 2007; Soriano et al., 2017). The full range of A is shown in Fig. 2a, which varies from -1 in CTC ($\alpha = 0$ & $b = 0$) to 1 in CTE ($\alpha = 90^\circ$ & $b = 1$). Correspondingly, $\phi(A)$ has the maximum value of 1 in CTC and minimum value of 0 in CTE. The physical significance is that the fibre-reinforcement effect is maximum in CTC and 0 in CTE, as bigger $\phi(A)$ makes χ and $\bar{p}^f$ bigger. Note that Eq. (14) gives no fibre-reinforcement in CTE with $\phi(A) = 0$, irrespective of F [Fig. 2(b)]. It is expected that for slightly anisotropic fibre orientation with small F, there should still be some fibre-reinforcement in CTE as significant amount of fibres can be oriented within the tensile strain domain. However, existing experiments show that the FRS samples prepared through vertical compaction typically have highly anisotropic fibre orientation which makes the fibre-reinforcement negligible in CTE (Diambra et al., 2007; Soriano et al., 2017; Mandolini et al., 2018). Therefore, Eq. (14) is employed in the present model. More general forms of Eqs. (13) and (14) are presented in Appendix 1, which can account for the effect of F.

It should be mentioned that the anisotropy of the sand is neglected in this modelling development. In fact, previous research seems to suggest that adopting an isotropic sand model is enough for modelling the anisotropic mechanical behaviour of FRS, since the anisotropic contribution of the fibre orientation has a much more dominant role (Diambra et al., 2010; Diambra et al., 2013). In addition, the account for the any anisotropy of the sand fabric will result in considerable increase in model complexity and required model parameters which may not be justified by the improvement in simulating FRS behaviour.

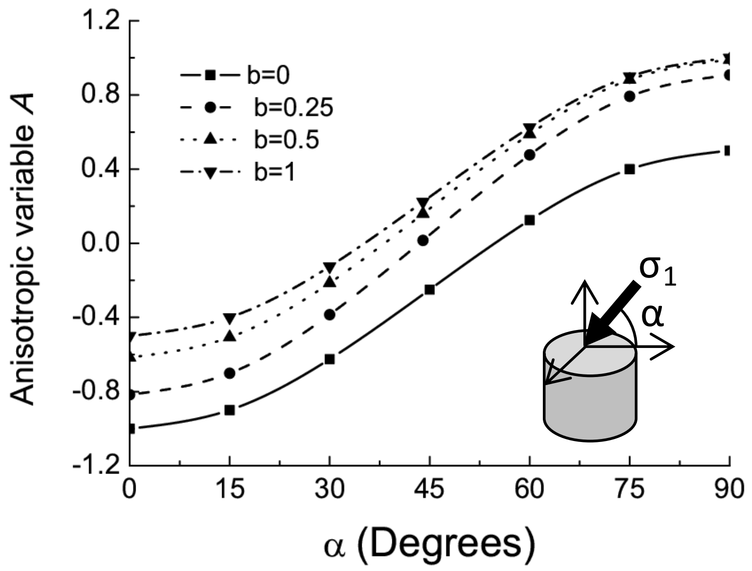

(a)

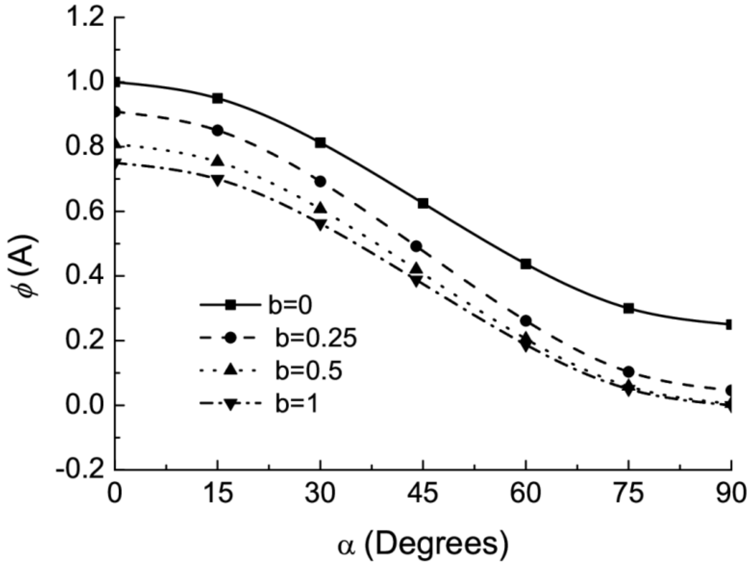

(b)

Fig. 2 Variation of the anisotropic variable A with α at different intermediate principal stress ratio b

3.4 Fibre volume and effective skeleton void ratio e^s

The volume of fibres has negligible influence on the global soil void ratio e, as a very small amount of fibres are typically used in FRS (Diambra et al., 2013). However, the fibres perturb the internal structure of the sand skeleton by preventing the use of some voids during the deformation process. This feature was modelled using the stolen void ratio concept (Diambra et al., 2013; Muir Wood et al., 2016) consisting in the modification of the sand skeleton void ratio by assigning some voids to the fibre space. Following such framework, it is assumed that the effective skeleton void ratio

e^s is different from the global void ratio e. The difference between e^s and e is dependent on various factors, including the sample preparation method, fibre properties (e.g., stiffness and aspect ratio) and fibre content. In this model, the simple relation between e^s and e is assumed:

$$e^s = \left(1 + x\rho_f\right)e \tag{16}$$

where x is a model parameter which can be either negative or positive, depending on the sample preparation method.

4 A MULTIAXIAL CONSTITUTIVE MODEL FOR FIBRE-REINFORCED SAND

The FRS model is established based on the framework proposed by Li & Dafalias (2002) for pure sand. The yield function and flow rule for plastic shear strain increment is expressed in terms of the stress tensor σ_{ij}, which is the same as that in Li and Dafalias (2002). To account for the effect of fibre inclusion on mechanical behaviour of FRS, the rest model formulations, including the dilatancy relation, plastic hardening law and elastic moduli, are expressed in terms of the sand skeleton stress and volumetric variables σ_{ij}^s and e^s, which are influenced by the fibre-sand interaction mechanisms defined in the previous section. When there are no fibres in the soil, the FRS model becomes an isotropic model for pure sand, as $\sigma_{ij}^s = \sigma_{ij}$ and $e = e^s$.

4.1 Yield function and plastic flow rule

The yield function follows the original model for sand by Li & Dafalias (2002):

$$f = R/g(\theta) - \mathcal{R} = 0 \tag{17}$$

where R $\left(= \sqrt{\frac{3}{2}r_{ij}r_{ij}}\right)$ is the stress ratio with $r_{ij} = \frac{s_{ij}}{p} = \left(\sigma_{ij} - p\delta_{ij}\right)/p$, $\mathcal{R}$ is a hardening parameter whose evolution law will be given in the subsequent section, $g(\theta)$ is an interpolation function based on the Lode angle θ of r_{ij} (or s_{ij}) as follows (Li and Dafalias, 2002):

$$g(\theta) = \frac{\sqrt{(1+c^2)^2 + 4c(1-c^2)sin3\theta} - (1+c^2)}{2(1-c)sin3\theta} \tag{18}$$

where c $(= M_e/M_c)$ is the ratio between the critical state stress ratio in triaxial extension M_e and that in triaxial compression M_c for the host sand. Note that this yield function neglects the plastic deformation under loading conditions with constant stress ratio R (e.g., isotropic or one-dimensional consolidation.

The plastic deviatoric strain increment is expressed as:

$$de_{ij}^{p} = \langle L \rangle n_{ij} \tag{19}$$

where L is the loading index and n_{ij} is the loading direction tensor defined as:

$$n_{ij} = \frac{\frac{\partial f}{\partial r_{ij}} - \left(\frac{\partial f}{\partial r_{mn}}\delta_{mn}\right)\delta_{ij}/3}{\left\| \frac{\partial f}{\partial r_{ij}} - \left(\frac{\partial f}{\partial r_{mn}}\delta_{mn}\right)\delta_{ij}/3 \right\|} \tag{20}$$

The total plastic strain increment $d\varepsilon_{ij}^{p}$ is (Li & Dafalias, 2002; Gao et al., 2014):

$$d\varepsilon_{ij}^{p} = de_{ij}^{p} + \frac{1}{3}d\varepsilon_{v}^{p}\delta_{ij} = \langle L \rangle \left(n_{ij} + \sqrt{\frac{2}{27}} D\delta_{ij} \right) = \langle L \rangle \mathrm{N}_{ij} \tag{21}$$

where the definition of N_{ij} is self-evident, $d\varepsilon_{v}^{p}$ is the plastic volumetric strain increment and D is the dilatancy relation expressed as:

$$D = \frac{d\varepsilon_{v}^{p}}{d\varepsilon_{q}^{p}} = \frac{d\varepsilon_{v}^{p}}{\sqrt{\frac{2}{3} de_{ij}^{p} de_{ij}^{p}}} \tag{22}$$

The rest of the model formulations (plastic hardening law, dilatancy relation and elastic moduli of FRS) is still based on the framework by Li & Dafalias (2002) but, in order to account for the effect of fibre stress and volumetric contributions, the modelling ingredients will be expressed with respect to stress and volumetric variables of the sand skeleton phase σ_{ij}^{s} and e^{s}.

4.2 Plastic hardening law

Based on the plastic hardening law for pure sand (Li & Dafalias, 2002; Gao et al., 2014), the following hardening law (evolution of $\mathcal{R}$) for FRS is proposed:

$$d\mathcal{R} = \langle L \rangle r_h = \frac{G(1-\zeta e^{s})}{p^{s}R^{s}} \left[M_c g(\theta^{s}) e^{-n\psi^{s}} - R^{s} \right] \tag{23}$$

where ζ and n are two model parameters, $R^{s} = \sqrt{\frac{3}{2} r_{ij}^{s} r_{ij}^{s}}$ with $r_{ij}^{s} = s_{ij}^{s}/p^{s} = \left(\sigma_{ij}^{s} - p^{s}\delta_{ij}\right)/p^{s}$ and $p^{s} = \sigma_{ii}^{s}/3$; $g(\theta^{s})$ is obtained using Eq. (18) by replacing θ with θ^{s} [$g(\theta^{s})$ is essentially the same as $g(\theta)$, as $s_{ij}^{s} = s_{ij}$]; ψ^{s} $(= e^{s} - e_c)$ is the state parameter (Been & Jefferies, 1985), with e_c being the critical state void ratio for the sand corresponding to the current p^s. The critical state line in the $e^s - p^s$ plane is given by (Li & Wang, 1998):

$$e_c = e_\Gamma - \lambda_c (p^s/p_a)^\xi \tag{24}$$

where e_Γ, λ_c and ξ are three material constants. Eq. (23) indicates that $d\mathcal{R} = 0$ when $R^s = M_c g(\theta^s) e^{-n\psi^s}$. This means that the fibre-reinforced sand can reach a ''virtual'' peak or bounding stress ratio $R_p^s = M_c g(\theta^s) e^{-n\psi^s}$, dependent on the current state of stress, void ratio and fibre orientation. This idea has been used in many sand models (Li and Dafalias, 2002; Taiebat and Dafalias, 2008; Li and Dafalias, 2012; Loukidis and Salgado, 2011; Woo and Salgado, 2015).

The dilatancy relation is expressed as:

$$D = d\left[M_c g(\theta^s) e^{m\psi^s} - R^s\right] \tag{25}$$

where d and m are two model parameters.

4.3 Elastic stress-strain relationship

The following empirical pressure-sensitive elastic moduli are employed for this model (Richart et al., 1970; Li & Dafalias, 2000; Gao et al., 2014):

$$G = G_0 \frac{(2.97 - e^s)^2}{1 + e^s} \sqrt{p^s p_a} \qquad \text{and} \qquad K = G \frac{2(1+\nu)}{3(1-2\nu)} \tag{26}$$

where G_0 is a material constant and ν is the Poisson's ratio. In conjunction with Eq. (26), the following hypoelastic stress-strain relationship is assumed for calculating the incrementally reversible deviatoric and volumetric strain increments de_{ij}^e and $d\varepsilon_v^e$:

$$de_{ij}^e = \frac{ds_{ij}}{2G} \quad \text{and} \quad d\varepsilon_v^e = \frac{dp}{K} \tag{27}$$

4.4 The constitutive equations

The condition of consistency of the yield function (Eq. 17) is:

$$df = \frac{\partial f}{\partial \sigma_{ij}} d\sigma_{ij} + \frac{\partial f}{\partial \mathcal{R}} d\mathcal{R} = \frac{\partial f}{\partial \sigma_{ij}} d\sigma_{ij} - \langle L \rangle r_h = 0 \tag{28}$$

Based on the additive decomposition of the strain increment $d\varepsilon_{ij} = d\varepsilon_{ij}^e + d\varepsilon_{ij}^p$, Eqs. (21) and (27) one can get:

$$d\sigma_{ij} = E_{ijkl}[d\varepsilon_{kl} - \langle L\rangle \mathrm{N}_{kl}] \tag{29}$$

where E_{ijkl} is the elastic stiffness tensor expressed as:

$$E_{ijkl} = (K - 2G/3)\delta_{ij}\delta_{kl} + 2G\delta_{ik}\delta_{jl} \tag{30}$$

The plastic loading index can then be obtained based on Eqs. (26)-(29) as:

$$L = \frac{\frac{\partial f}{\partial \sigma_{ab}} E_{abkl}}{r_H + \frac{\partial f}{\partial \sigma_{mn}} E_{mnpq}\mathrm{N}_{pq}} d\varepsilon_{kl} = \Pi_{kl} d\varepsilon_{kl} \tag{31}$$

Using Eqs. (29) and (31), by standard procedure in plasticity one obtains the incremental stress-strain relationship:

$$d\sigma_{ij} = \Lambda_{ijkl} d\varepsilon_{kl} \tag{32}$$

with the elastoplastic stiffness tensor Λ_{ijkl} being expressed as:

$$\Lambda_{ijkl} = E_{ijkl} - h(L)E_{ijmn}\mathrm{N}_{mn}\Pi_{kl} \tag{33}$$

where $h(L)$ is the Heaviside step function, with $h(L > 0) = 1$ and $h(L \geq 0) = 0$. The full expression for $\frac{\partial f}{\partial \sigma_{ij}}$ is provided in Appendix 2. When there is no fibre in the soil, the model becomes an isotropic model for sand with state-dependent dilatancy.

Based on the present model formulations, the soil will eventually reach the critical state with constant stress, constant void ratio and constant p^f which describes the fibre-reinforcement to soil strength. There will be unique critical state lines (CSLs) in the $p^s - q^s$ and $e^s - p^s$ planes for FRS, with $q^s = q$. The slope of the CSL in the $p^s - q^s$ plane is dependent on the Lode's angle but neither of the CSLs is affected by the loading direction. However, this does not mean unique CSLs in the $p - q$ and $e - p$ planes for FRS, because p^s is expressed in terms of p^f (Eq. 5), which is dependent on the loading direction (Eqs. 2, 4 and 14). When there is no fibres, the model becomes an isotropic model for sand which gives unique CSLs in the $p - q$ and $e - p$ planes, irrespective of the loading direction (Li and Dafalias, 2002; Taiebat and Dafalias, 2008; Li and Dafalias, 2012; Loukidis and Salgado, 2011; Woo and Salgado, 2015). More research should be done to find out if this assumption represents the reality. But it is generally very difficult to shear FRS to the critical state in a laboratory test, because p^f may reach a steady state value at very large strains in some cases (Diambra et al., 2010). At that strain level, deformation of the sample is always highly ununiform, which makes the measurement of critical state difficult. Numerical modelling, for example using the discrete element technique may offer some insight on this matter.

5. MODEL VALIDATION AGAINST MULTIAXIAL TESTS

5.1 Experimental data and conditions

There is very little test data on the mechanical behaviour of FRS under multiaxial loading conditions. Mandolini et al. (2018) were the first to report a series of drained hollow cylinder torsional tests on Hostun sand (S28) reinforced with Loksand™ polypropylene fibres. Hostun sand has a specific gravity G_s =2.65 and maximum e_{max} and minimum e_{min} void ratios of 1.0 and 0.63, respectively. The polypropylene fibres used in these tests are 17.5 mm long and 0.1 mm in diameter with a specific gravity G_f=0.91. A fibre weight content w_f of 0.5% was used for all fibre reinforced samples.

Unreinforced and fibre-reinforced samples have been sheared to failure by imposing different orientation of the major principal stress axis (α) with respect to the preferred horizontal bedding fibres. Testing was carried out by imposing the same internal and external cell confining pressures which were kept constant at σ_c (100 kPa or 200 kPa) during the whole test duration. Under these pressure conditions, the intermediate stress ratio b remains constant and is expressed as $b = \sin^2\alpha$.

5.2 Determination of the fibre orientation and model parameters

The current constitutive model requires the definition of fifteen model parameters. Eleven parameters are necessary for the baseline constitutive model for the sand while only four additional parameters (χ_r, κ, μ and x) are introduced to account for the effect of the fibre reinforcement. Description of the fibre orientation distribution is also required.

The calibration of the parameter for the baseline model is carried out following the general procedure detailed by Li & Dafalias (2002) and using data for unreinforced sands. Note that most of the parameters for pure sand are determined using the test data with $\alpha = 0°$ and $\alpha = 15°$, while c is determined based on the failure stress ratio of sand at $\alpha = 90°$ $(b = 1)$. The four parameters for FRS and the model ingredients linked to the fibre orientation are determined following the steps below:

(a) First, it is necessary to define the fibre orientation tensor H_{ij} and, most importantly its deviatoric part F_{ij} which is used in the model formulations. Based on the measured fibre orientation in the FRS (Diambra et al. 2007, Soriano et al. 2017) the parameters for Eq. (11) are obtained as $\rho_0 = 0$, $\rho_a = 0.35$ and $k = 6$. Employing Eqs. (8) and (12), a value of $F = 0.26$ for the deviatoric tensor F_{ij} defined in Eq (13) can be determined.

(b) χ_r and κ are determined using Eqs. (1) and (4) and the peak stress states in CTC. Specifically, χ_r and κ are calibrated to make Eq. (1) best fit the peak stress states of the two triaxial compression tests with $\alpha = 0^{\circ}$ and $b = 0$(Fig. 3). Note that $\chi_r = \chi$ in CTC as $\phi(A) = 1$.

(c) The complete stress-strain relationship is needed for determining μ and x. For the tests with $\alpha = 90^{\circ}$ [$b = 1$ for the loading conditions in Mandolini et al., (2018)], there is no fibre-reinforcement to the soil strength [$\phi(A) = 0$ in Eq. 15 and Fig. 2b], which means that $p_f = 0$ and μ has no influence on the stress-strain relationship of FRS. Therefore, the $\varepsilon_q - \varepsilon_v$ relationship for the test $\sigma_c = 200\ \mathrm{kPa}$ with $\alpha = 90^{\circ}$ is used to determine the value of x first. μ is then determined based on the deviatoric stress-strain relation in a CTC test with $\alpha = 0^{\circ}$ and $b = 0$ with the x obtained. Fig. 4 indicates that $\mu = 9.5$ and $x = -2$ provides a reasonable simulation of the experimental data.

The values of the calibrated parameters are summarised in Table 1. The remaining tests are used for validating the model performance.

5.3 Model simulations

Comparisons of the complete stress-strain relationship between the model simulations (full lined) and the experimental test results by Mandolini et al. (2018) (dotted lines) are shown in Figs. 5 to 10. It is evident that the peak q decreases as α increases at the same σ_c, which is due to the anisotropy of fibre orientation. Once $\alpha \geq 60°$, the fibre-reinforcement to sand strength becomes very small, as $\phi(A)$ reaches a small value. This is well captured by the proposed model. In some tests, however, the model gives lower q than measured (Figs. 5c and 7c). While this discrepancy could be caused by the model itself, some experimental variability and development of shear bands in the samples may also have played a role. Therefore, it can be concluded that the expressions for $\phi(A)$ in Eqs. (14) and (15) are sufficient for modelling the strength anisotropy of this FRS. For more general cases, Eqs. (34) and (35) presented in Appendix 1 may have to be used for modelling the strength of FRS with low degree of fibre orientation anisotropy.

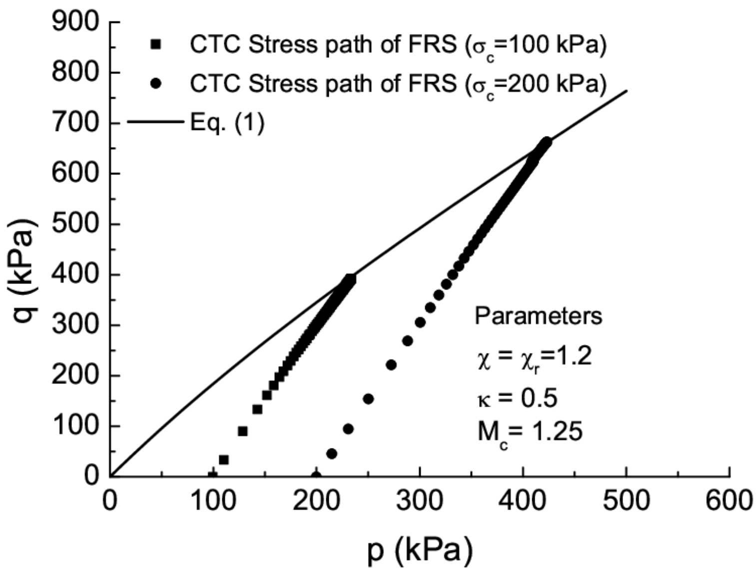

Fig. 3 Determination of parameters χ_r and κ

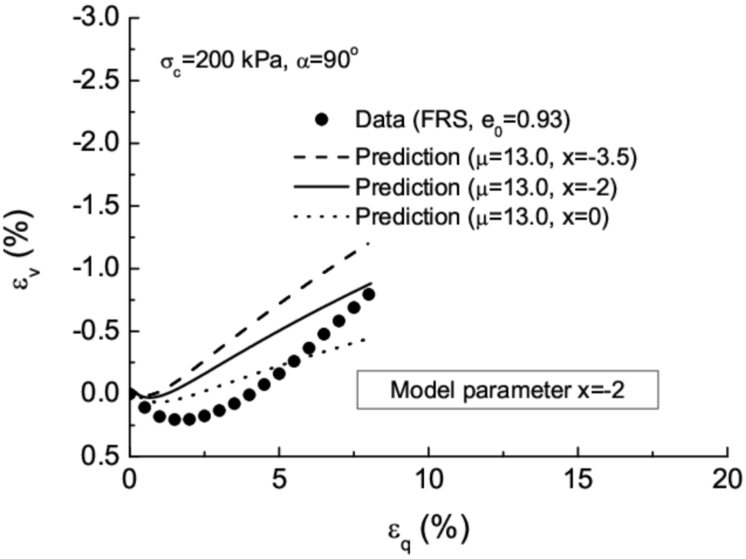

(a)

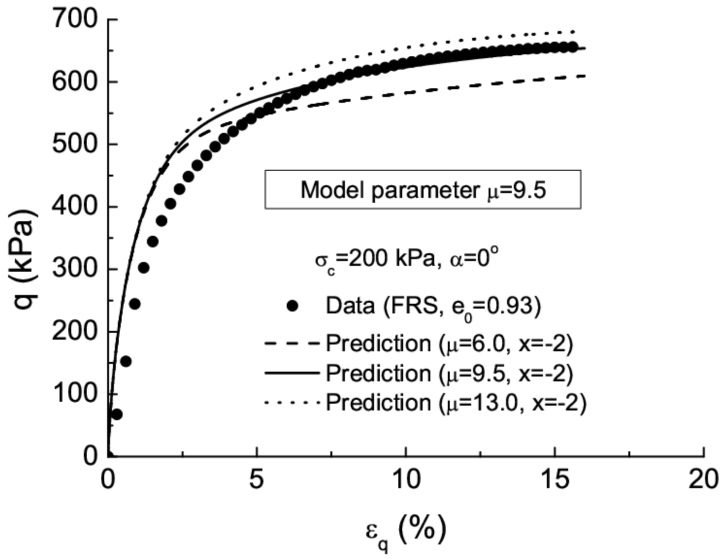

(b)

Fig. 4 Determination of preliminary values for x and μ

Table 1 Model parameters for fibre-reinforced Hostun RF (S28) sand

Critical state	Elasticity	Plastic hardening and dilatancy	Fibre-reinforcement
$M_c = 1.25$	$G_0 = 120$	$n = 1.5$	$\chi_r = 1.2$
$c = 0.75$	$\nu = 0.2$	$\zeta = 0.2$	$\kappa = 0.6$
$e_\Gamma = 0.98$		$d = 1.0$	$\mu = 9.5$
$\lambda_c = 0.01$		$m = 1.0$	$x = -2.0$
$\xi = 0.7$			

The volumetric behaviour is generally well captured with an increased dilative response for FRS if compared to the respective unreinforced samples. This is an effect of the introduced correction to the sand matrix void ratio as per the stolen void ratio concept. However, some discrepancies between the simulated and experimental volumetric response are still visible (e.g. Fig. 5b and 6b) and they may be exacerbated by small inaccuracy in the experimental determination of the actual void ratio (small variations of soil density have a large effect on the volumetric response, see for example Diambra et al. (2010)) or strain localisation and inhomogeneous deformation which may appear in the thin walled hollow cylindrical samples, as discussed in Mandolini et al. (2018). Meanwhile, Figs. 8 and 10 show that the model underestimates the volume contraction of pure sand. One can get more satisfactory prediction of sand behaviour for these loading conditions by using an anisotropic sand model with more parameters (Li and Dafalias, 2002; Li and Dafalias, 2012). But this may not lead to better prediction of FRS behaviour as well, which is of more importance for geotechnical problems involving FRS.

Fig. 11 shows the model prediction for the failure of FRS at different σ_c. Since no obvious peak of q has been observed in some tests (e.g., Figs. 5), the failure stress state is defined as that at $\varepsilon_q = 10\%$ (Mandolini et al. 2018). The model is found to give good prediction for the tests with $\sigma_c = 100\ \mathrm{kPa}$ (Fig. 11a), with slight overestimation for FRS at $\alpha = 15^\circ$ and 30°. For the tests with $\sigma_c = 200\ \mathrm{kPa}$, the model prediction is in good agreement with the test data at $\alpha = 0^\circ, 15^\circ$, 30° and 90° but is higher than the measured strength for $\alpha = 45^\circ$ and 60°. This could be due to the strain localization in the samples (Mandolini et al. 2018). Note that the test on FRS with $\alpha = 60^\circ$ and $\sigma_c = 200\ \mathrm{kPa}$ was not carried out with exactly the same α during the test, which makes the test data deviate from the line of $\alpha = 60^\circ$, but the experimental value still agree with the predicted deviatoric envelope (Fig. 11b).

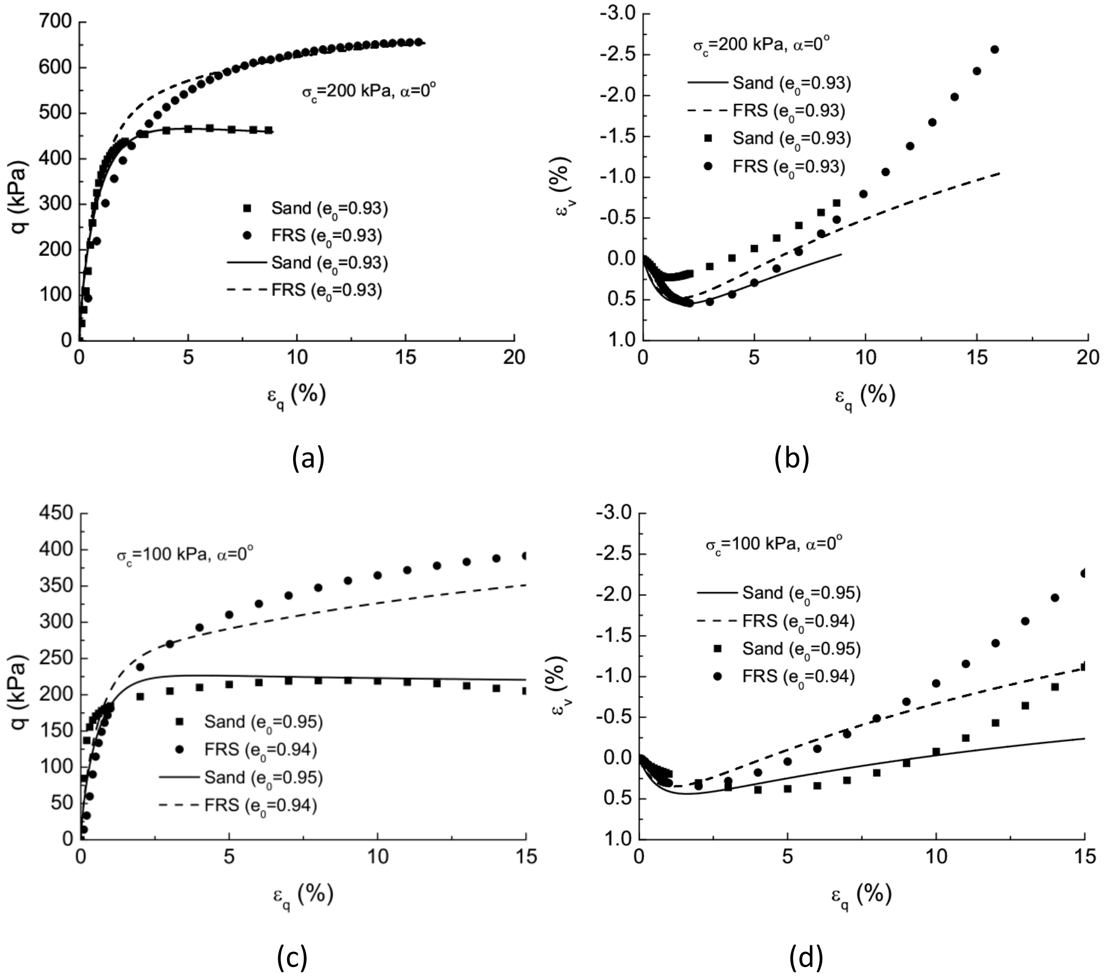

Fig. 5 Comparison between the test data and model simulations for the stress-strain relationship of fibre-reinforced Hostun RF (S28) sand at $\alpha = 0^{\circ}$ (data from Mandolini et al., 2018)

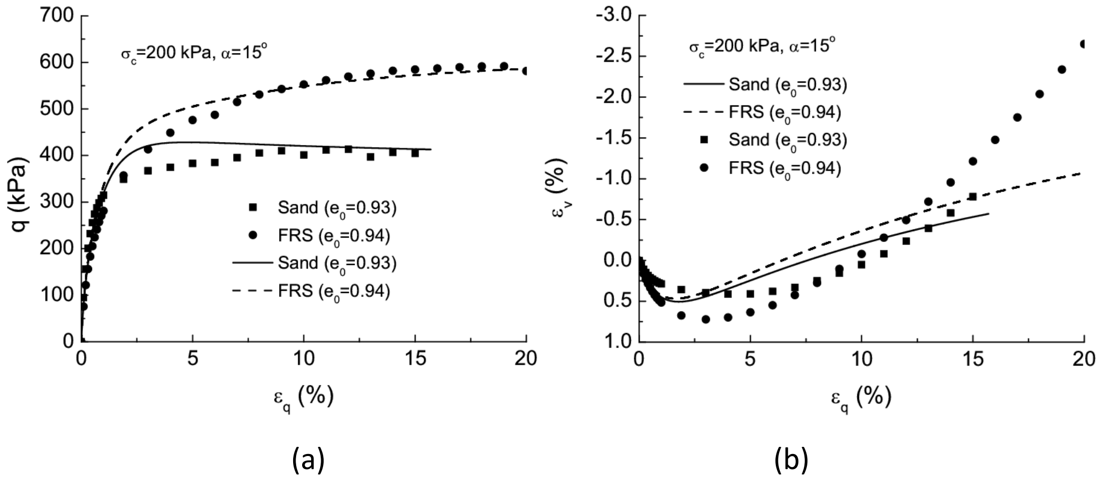

Fig. 6 Comparison between the test data and model simulations for the stress-strain relationship of fibre-reinforced Hostun RF (S28) sand at $\alpha = 15^{\circ}$ (data from Mandolini et al., 2018)

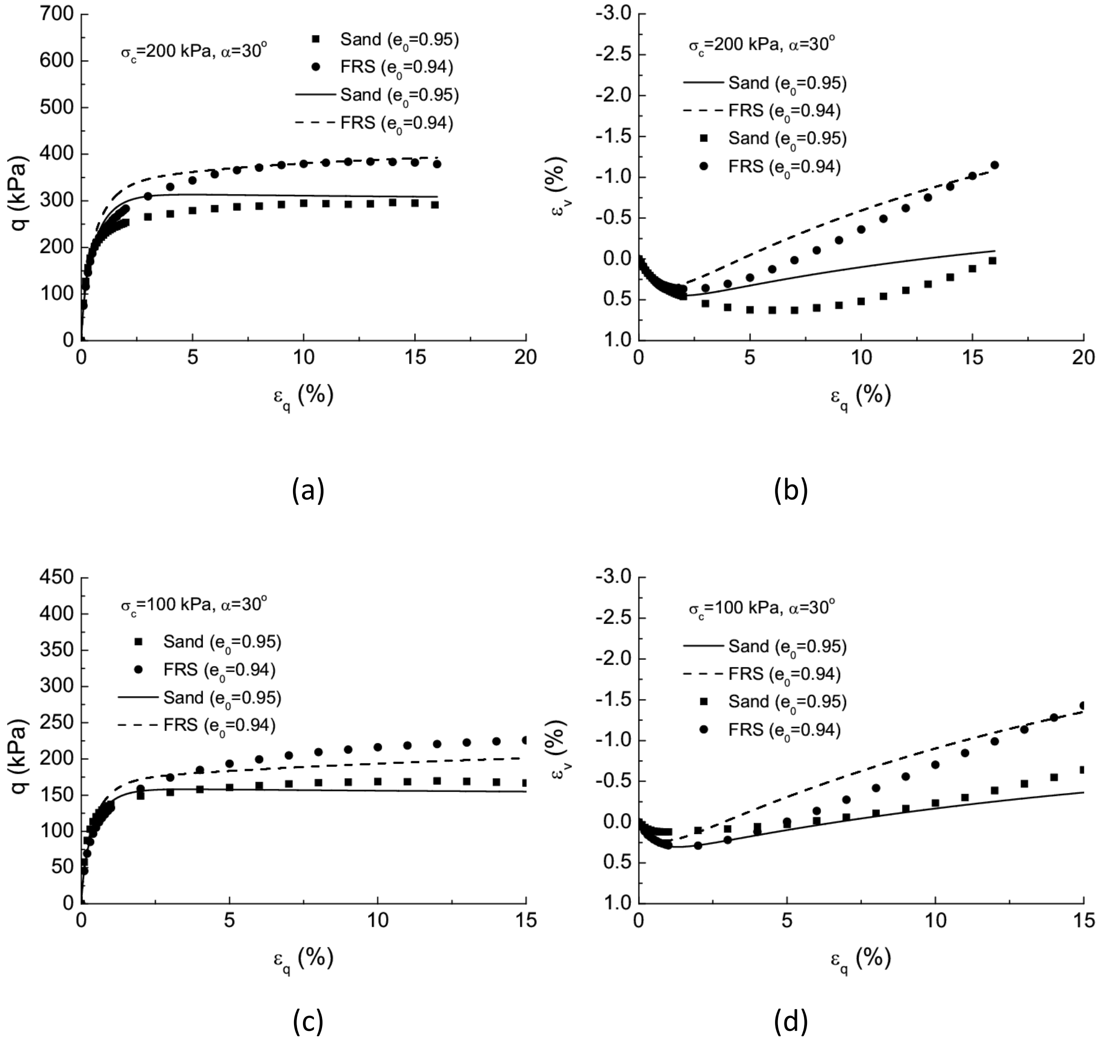

Fig. 7 Comparison between the test data and model simulations for the stress-strain relationship of fibre-reinforced Hostun RF (S28) sand at $\alpha = 30^{\circ}$ (data from Mandolini et al., 2018)

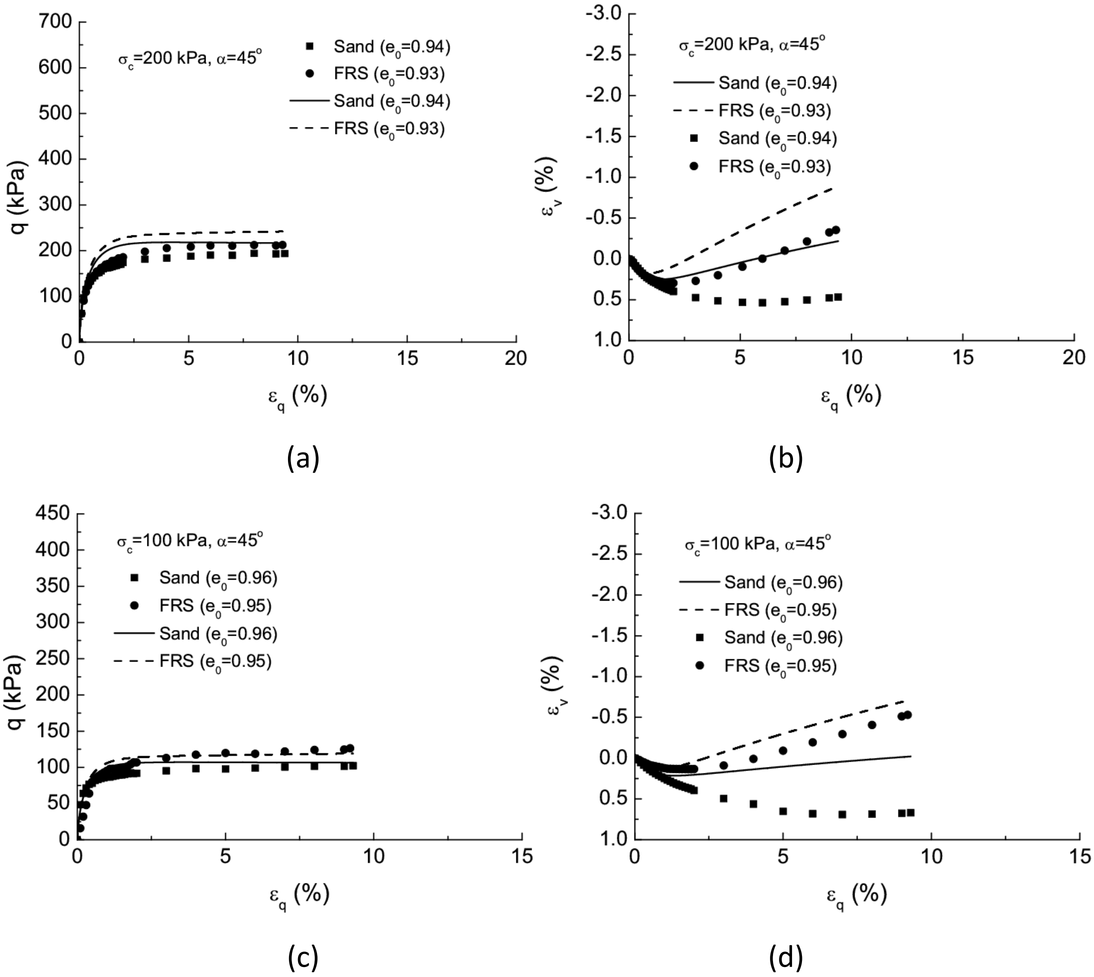

Fig. 8 Comparison between the test data and model simulations for the stress-strain relationship of fibre-reinforced Hostun RF (S28) sand at $\alpha = 45^{\circ}$ (data from Mandolini et al., 2018)

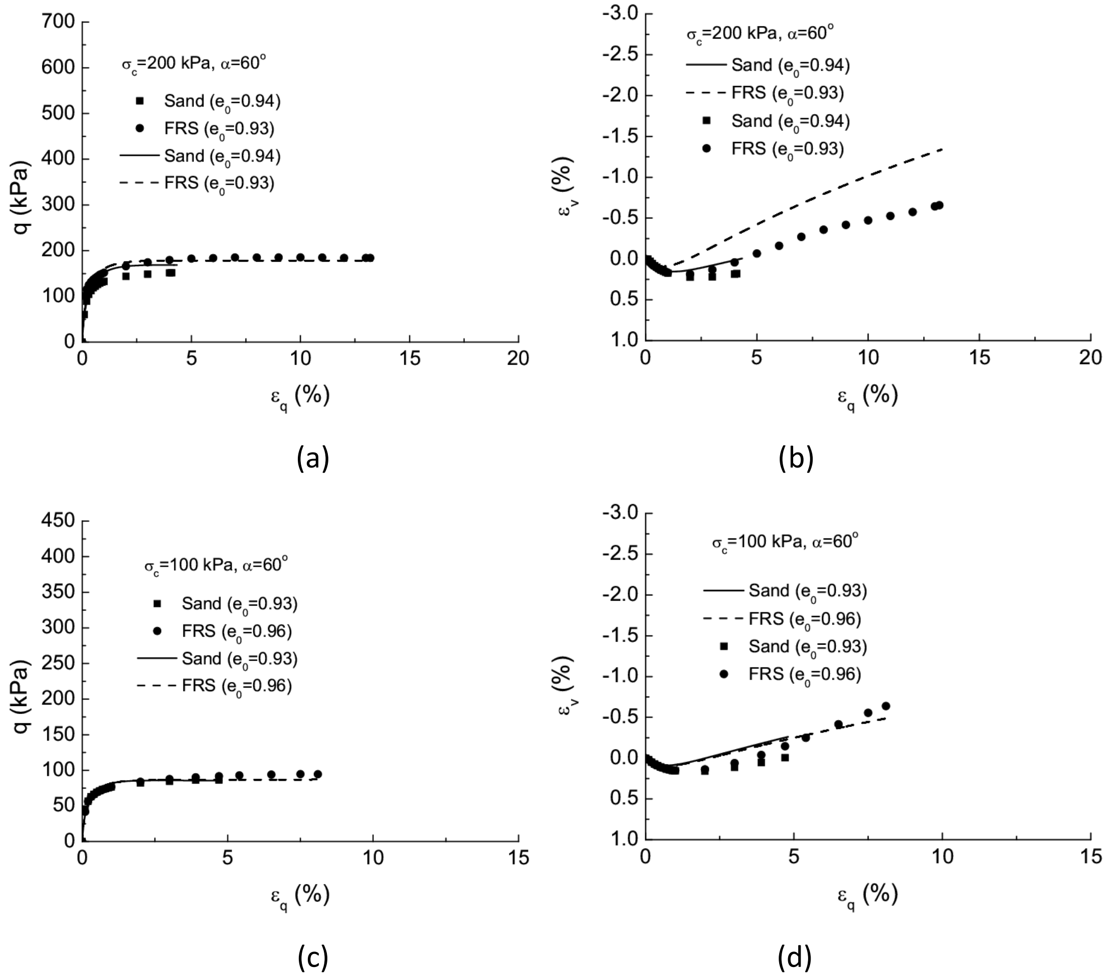

Fig. 9 Comparison between the test data and model simulations for the stress-strain relationship of fibre-reinforced Hostun RF (S28) sand at $\alpha = 60^{\circ}$ (data from Mandolini et al., 2018)

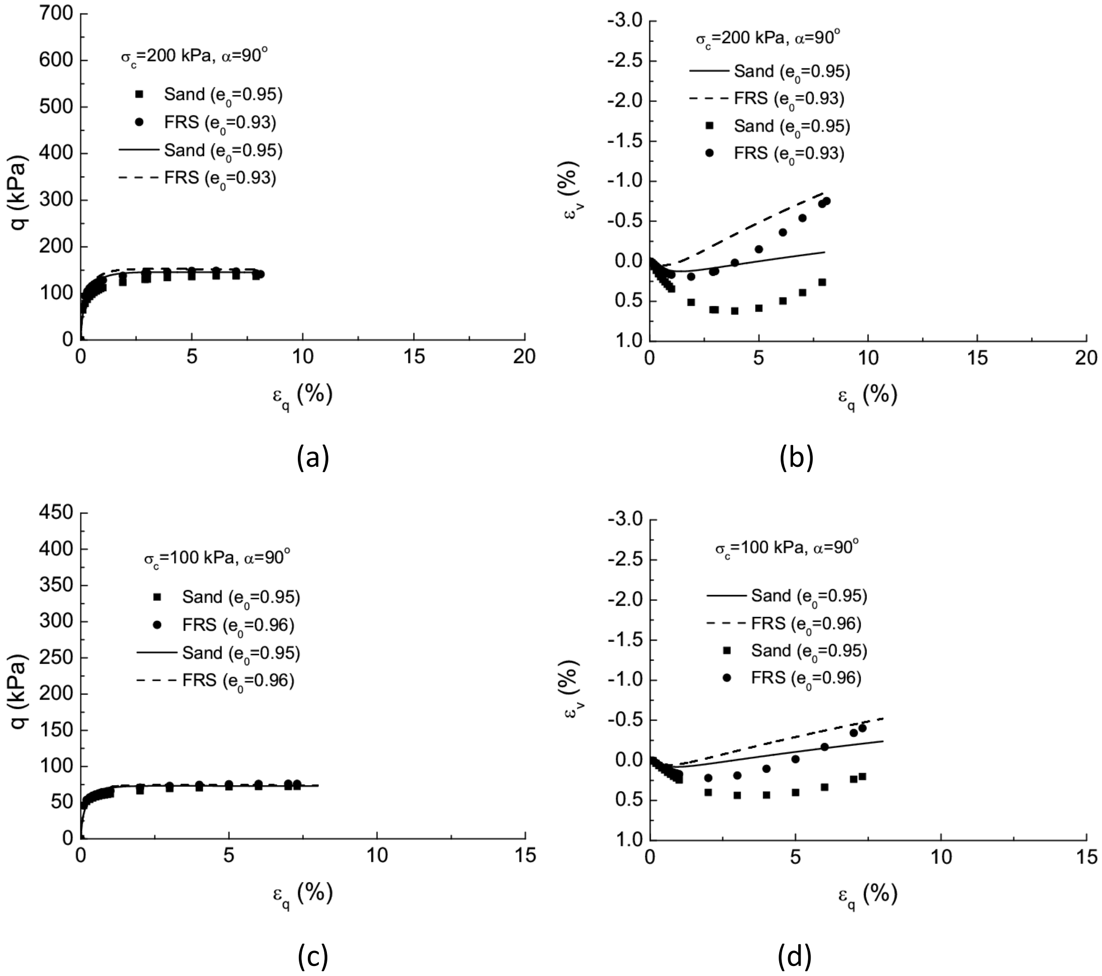

Fig. 10 Comparison between the test data and model simulations for the stress-strain relationship of fibre-reinforced Hostun RF (S28) sand at $\alpha = 90^{\circ}$ (data from Mandolini et al., 2018)

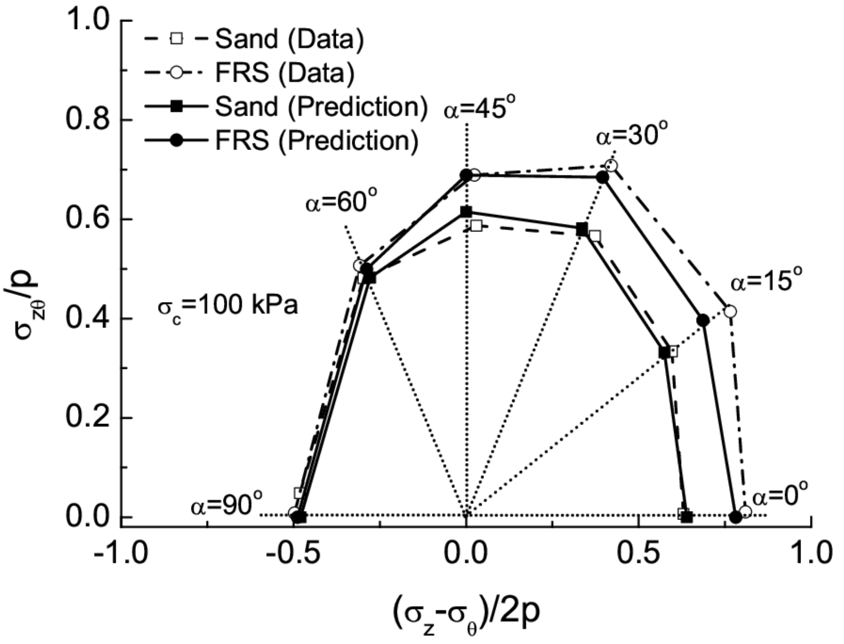

(a)

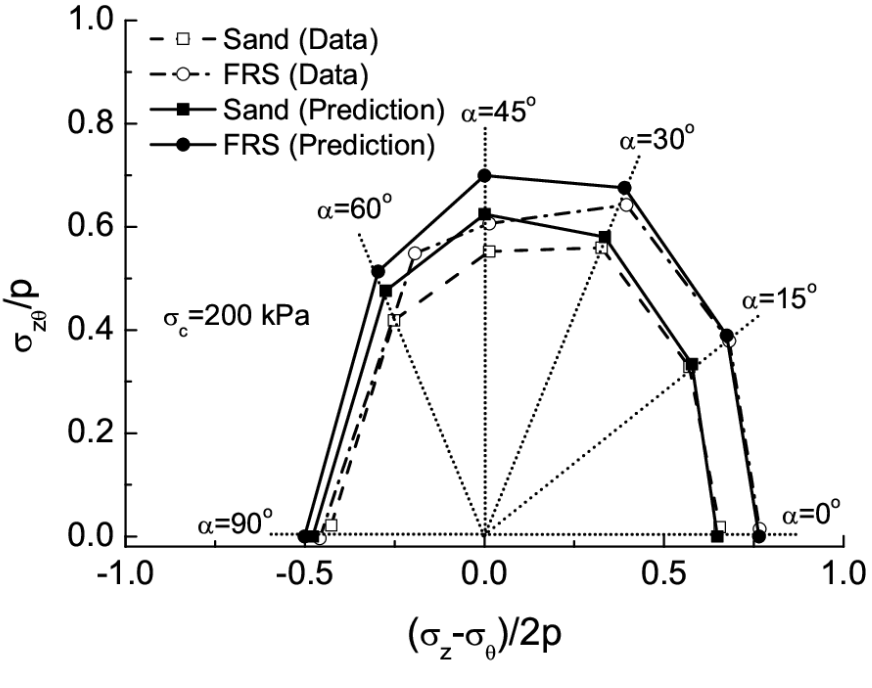

(b)

Fig. 11 Comparison between the test data and model prediction for the strength of fibre-reinforced Hostun RF (S28) at (a) $\sigma_c = 100\ \mathrm{kPa}$ and (b) $\sigma_c = 200\ \mathrm{kPa}$. Failure stress state is defined as that at $\varepsilon_q = 10\%$ (Mandolini et al., 2018)

6. CONCLUSIONS

Mechanical behaviour of FRS is affected by the anisotropic orientation of fibres within the host soil. The reinforcement contribution of the fibre to the sand strength is higher when more fibres are oriented in the direction of tensile strains. This study presents the first multiaxial constitutive model for FRS, which has the following features:

(a) The proposed modelling framework treats the fibre reinforced soil as a unique composite material and builds on the well-established constitutive modelling framework by Li & Dafalias (2002). It is assumed that, while the yield function is expresses in term of the current overall stress, the main modelling ingredients (hardening rule, elastic properties, dilatancy and failure) are governed by the stress and density of the sand skeleton, which are both affected by the stress and density contributions of the fibres.

(b) The stress contribution of the fibres, affecting the stress experienced by the sand skeleton σ_{ij}^{s}, is assumed to evolve with the deformation experienced by the sand skeleton. The anisotropic nature of the fibre stress contribution is further modelled through an anisotropic variable A, expressed in terms of a joint invariant of the loading direction tensor n_{ij} and deviatoric fibre orientation tensor F_{ij}, which governs the value of the isotropic fibre stress at failure.

(c) The density contribution of the fibres is modelled by a modification of the void ratio of the sand skeleton, following the previously established stolen void ratio concept (Wood et al., 2016).

Compared to the baseline sand constitutive model by Li & Dafalias (2002), four additional parameters are introduced to characterize the effect of fibre inclusion on mechanical response of FRS. These parameters can be readily determined using triaxial test data. The model has been used to simulate the stress-strain relationship of FRS tested under multiaxial stress condition in the hollow cylinder torsional apparatus. Good agreement between the model simulations and test results is observed. In particular, the model gives satisfactory prediction for the strength anisotropy of FRS under multiaxial loading condition. Future improvement of the model regarding the general expressions of Eqs. (14) and (15) is discussed in Appendix 1.

ACKNOWLEDGEMENTS

The authors would like to thank the support of the Engineering and Physical Sciences Research Council (EPSRC) grant EP/J010022/1 under which the experimental tests were performed.

APPENDIX 1: More general forms of Eqs. (14) and (15)

A general expression for χ_r should be expressed in terms of both F and ρ_f, as the fibre-reinforcement effect is affected by both fibre content and fibre orientation anisotropy (Michalowski and Čermák, 2002; Michalowski, 2008; Diambra et al., 2013; Mandolini et al., 2018). Variation of the fibre-reinforcement with loading direction is dependent on not only A but also on F in general. Bigger F makes ϕ decrease faster as A increases (Michalowski and Čermák, 2002; Michalowski, 2008). Therefore, a general expression of Eqs. (13) should be

$$\chi = \chi_r(\rho_f, F)\phi(A, F) \tag{34}$$

A proper expression for where χ_r is difficult to propose at present, because there is insufficient test data on FRS with various combinations of F and ρ_f. However, some existing analytical methods (Michalowski and Čermák, 2002; Diambra et al., 2013) and numerical methods (Sivakumar Babu et al., 2008) can help such development. A simple form of ϕ can be expressed as

$$\phi(A, F) = \langle 1 - \frac{F}{2F_c}(1 + A) \rangle \tag{35}$$

where F_c is a critical degree of fibre orientation anisotropy and $\langle\ \ \rangle$ are used to ensure $\phi \geq 0$. It is physically unreasonable to have negative ϕ, because it would indicate that fibre inclusion can reduce the sand strength according to Eqs. (1) and (4). Eq. (33) has the following features: (a) $\phi(A, F)$ has the maximum value of 1 at in

CTC with $A=-1$ and the minimum value of $\langle 1-\frac{F}{F_c}\rangle$ in CTE with $A=1$. When $F\geq F_c$, no fibre-reinforcement in CTE is predicted as $\phi(A)=0$ for this loading condition. This essentially means that most FRS prepared in the laboratory has $F\geq F_c$; (b) $\phi(A)=1$ for isotropic fibre orientation with $F=0$, which means that fibre-reinforcement is independent of the loading (or strain increment) direction. When F is much bigger than F_c, $\phi(A)$ can reach 0 when $A<1$. More experimental and numerical work would be required to validate the proposed Eq. (35).

APPENDIX 2: Partial differential equations

The expression for $\frac{\partial f}{\partial \sigma_{ij}}$ is

$$\frac{\partial f}{\partial \sigma_{ij}}=\frac{\partial f}{\partial r_{kl}}\frac{\partial r_{kl}}{\partial \sigma_{ij}} \tag{36}$$

where (Li and Dafalias, 2002)

$$\frac{\partial f}{\partial r_{kl}}=\frac{3}{2R^2g^2(\theta)}\left\{\left[Rg(\theta)+3Rsin3\theta\frac{\partial g(\theta)}{\partial sin3\theta}\right]r_{kl}+\frac{\partial g(\theta)}{\partial sin3\theta}r_{km}r_{lm}\right\} \tag{37}$$

$$\frac{\partial g(\theta)}{\partial sin3\theta}=\frac{c(1+c)}{sin3\theta\sqrt{(1+c^2)^2+4c(1-c^2)sin3\theta}}-\frac{g(\theta)}{sin3\theta} \tag{38}$$

$$\frac{\partial r_{kl}}{\partial \sigma_{ij}}=\frac{\delta_{ki}\delta_{lj}}{p}-\frac{\sigma_{kl}\delta_{ij}}{3p^2} \tag{39}$$

LIST OF NOTATIONS

A	Anisotropic variable
D	Dilatancy equation
e	Void ratio
e^s	Skeleton void ratio
e_{ij}^e and e_{ij}^p	Elastic and plastic deviatoric strain
F	Degree of fibre orientation anisotropy
F_{ij}	Deviatoric fibre orientation tensor
f	Yield function

G	Elastic shear modulus
H_{ij}	Fibre orientation tensor
$g(\theta)$	Interpolation function for the critical state stress ratio
K	Elastic bulk modulus
M_c, M_e	Critical state stress ratio in triaxial compression and triaxial extension
$p,\ p^s$	Mean stress and skeleton mean stress
R	Stress ratio
r_{ij}	Stress ratio tensor
s_{ij}	Deviatoric stress tensor
α	Angle between the major principal stress and direction of deposition
δ_{ij}	Kronecker delta
ε_{ij}	Total strain tensor
ρ_f	Volume fraction of fibres
θ	Lode angle of the stress tensor
$\sigma_{ij},\ \sigma_{ij}^s$	Stress tensor and skeleton stress tensor
ψ^s	State parameter for fibre-reinforced sand

REFERENCES

Consoli, N. C., Heineck, K. S., Casagrande, M. D. T., & Coop, M. R. (2007). Shear strength behavior of fiber-reinforced sand considering triaxial tests under distinct stress paths. *J. Geotech. Geoenviron. Eng.,* 133(11), 1466-1469. **doi**: 10.1061/(ASCE)1090-0241(2007)133:11(1466).

di Prisco, C. & Nova, R. (1993). A constitutive model for soil reinforced by continuous threads. *Geotext. Geomembr.*, **12**, No. 2, 161-178, **doi**: 10.1016/0266-1144(93)90004-8.

Diambra, A. and Ibraim, E. (2015). Fibre-reinforced sand: interaction at the fibre and grain scale. *Géotechnique*, **65**, No. 4, 296-308. **doi**: 10.1680/geot.14.P.206.

Diambra, A., & Ibraim, E. (2014). Modelling of fibre–cohesive soil mixtures. *Acta Geotechnica*, **9**, No. 6, 1029-1043. **doi**: 10.1007/s11440-013-0283-y.

Diambra, A., Ibraim, E., Russell, A. R., & Wood, D. M. (2013). Fibre reinforced sands: from experiments to modelling and beyond. *Int. J. Numer. Analyt. Meth. Geomech.,* **37**, No. 15, 2427-2455, **doi**: 10.1002/nag.2142.

Diambra, A., Ibraim, E., Wood, D. M. & Russell, A. R. (2010). Fibre reinforced sands: experiments and modelling. *Geotext. Geomembr.*, **28**, No. 3, 238-250, **doi**: 10.1016/j.geotexmem.2009.09.010.

Diambra, A., Russell, A. R., Ibraim, E. & Muir Wood, D. (2007). Determination of fibre orientation distribution in reinforced sands. *Géotechnique* **57**, No. 7, 623–628, **doi**: 10.1680/geot.2007.57.7.623.

Ding, D. & Hargrove, S. (2006). Nonlinear stress-strain relationship of soil reinforced with flexible geofibers. *J. Geotech. Geoenviron. Eng.,* **132**, No. 6, 791-794, **doi**: 10.1061/(ASCE)1090-0241(2006)132:6(791).

Festugato, L., Peccin da Silva, A., Diambra, A., Consoli, N.C. & Ibraim, E. (2018) Modelling tensile/compressive strength ratio of fibre reinforced cemented soils." *Geotextiles and Geomembranes,* **46**, No. 2: 155-165. **doi**: 10.1016/j.geotexmem.2017.11.003.

Gao, Z. W. & Zhao, J. D. (2013). Evaluation on failure of fibre-reinforced sand. *J. Geotech. Geoenvir. Engrg.,* **139**, No. 1, 95-106, **doi**: 10.1061/(ASCE)GT.1943-5606.0000737.

Gao, Z. W., Zhao, J. D., Li, X. S. & Dafalias, Y.F. (2014). A critical state sand plasticity model accounting for fabric evolution. *Int. J. Numer. Analyt. Meth. Geomech.,* **38**, No. 4, 370-390, **doi**: 10.1002/nag.2211.

Gao, Z.W., Zhao, J.D., Yao, Y.P. (2010). A generalized anisotropic failure criterion for geomaterials. International Journal of Solids and Structures. **47**, No. 22-23, 3166-3185. **doi**: 10.1016/j.ijsolstr.2010.07.016.

Gray, D. H. & Ohashi, H. (1983). Mechanics of fiber reinforcement in sands. *J. Geotech. Eng.,* **109**, No. 3, 335-353, **doi**: 10.1061/(ASCE)0733-9410(1983)109:3(335).

Li, X. S. & Dafalias, Y. F. (2000). Dilatancy for cohesionless soils. *Géotechnique*, **50**, No. 4, 449-460, **doi**: 10.1680/geot.2000.50.4.449.

Li, X. S. & Dafalias, Y. F. (2002). Constitutive modelling of inherently anisotropic sand behaviour. *J. Geotech. Geoenvir. Engrg.,* **128**, No. 10, 868-880, **doi**: 10.1061/(ASCE)1090-0241(2002)128:10(868).

Li, X. S. & Dafalias, Y. F. (2012). Anisotropic critical state theory: role of fabric. *J. Eng. Mech.,* **138**, No. 3, 263-275. **doi**: 10.1061/(ASCE)EM.1943-7889.0000324.

Loukidis, D. & Salgado, R. (2011). Effect of relative density and stress level on the bearing capacity of footings on sand. *Géotechnique*. **61**, No. 2, 107-119. **doi**: 10.1680/geot.8.P.150.3771.

Mandolini, A., Diambra, A. & Ibraim, E. (2018). Strength anisotropy of fibre-reinforced sands under multiaxial loading. *Géotechnique*, 1-14, **doi**: 10.1680/jgeot.17.P.102.

Michalowski, R. L. & Čermák, J. (2002). Strength anisotropy of fiber-reinforced sand. *Comput. Geotech.,* **29**, No. 4, 279-299, **doi**: 10.1016/S0266-352X(01)00032-5.

Michalowski, R. L. (1996). Micromechanics-based failure model of granular /particulate medium with reinforcing fibers. Technical Report, Air Force office of Scientific Research, USA.

Michalowski, R. L. (2008). Limit analysis with anisotropic fiber-reinforced soil. Géotechnique **58**, No. 6, 489-501, **doi**: 10.1680/geot.2008.58.6.489.

Michalowski, R. L. (2008). Limit analysis with anisotropic fibre-reinforced soil. *Géotechnique,* **58**, No. 6, 489-501, **doi**: 10.1680/geot.2008.58.6.489.

Ranjan, G., Vasan, R. M. & Charan, H. D. (1996). Probabilistic analysis of randomly distributed fiber-reinforced soil. *J. Geotech. Eng.,* **122**, No. 6, 419-426, **doi**: 10.1061/(ASCE)0733-9410(1996)122:6(419).

Richart, F. E. Jr., Hall, J. R. & Woods, R. D. (1970). Vibrations of soils and foundations. Englewood Cliffs, NJ: Prentice-Hall.

Santoni, R. L. & Webster, S. L. (2001). Airfields and road construction using fiber stabilization of sands. *J. Transp. Eng.,* **127**, No. 2, 96-104, **doi**:

10.1061/(ASCE)0733-947X(2001)127:2(96).

Shukla, S. K. (2017). Fundamentals of Fibre-Reinforced Soil Engineering. Springer Nature Singapore Pte Ltd.

Silva Dos Santos, A. P., Consoli, N.C., and Baudet, B. A. (2010). The mechanics of fibre-reinforced sand. *Géotechnique,* **61**, No. 10, 791-799, **doi**: 10.1680/geot.8.P.159.

Sivakumar Babu, G. L., Vasudevan, A. K. & Haldar, S. (2008). Numerical simulation of fiber-reinforced sand behaviour. *Geotext. Geomembr.,* **26**, No. 2, 181-188, **doi**: 10.1016/j.geotexmem.2007.06.004.

Sonnenberg R., Bransby M. F., Hallett P. D., Bengough A. G., Mickovski S. B. & Davies M. C. R. (2010). Centrifuge modelling of soil slopes reinforced with vegetation. *Can. Geotech. J.,* **47**, No. 12, 1415-1430, **doi**: 10.1139/T10-037.

Soriano, I., Ibraim, E., Andò, E., Diambra, A., Laurencin, T., Moro, P. & Viggiani, G. (2017). 3D fibre architecture of fibre-reinforced sand. Granular Matter, **19**, No. 4, 75. DOI: 10.1007/s10035-017-0760-3.

Tang, C.S., Shi, B., Cui, Y.J., Liu, C. & Gu, K. (2012). Desiccation cracking behaviour of polypropylene fibre–reinforced clayey soil. *Can. Geotech. J.,* **49**, No. 9, 1088-1101. **doi**: 10.1139/t2012-067.

Taiebat, M., & Dafalias, Y. F. (2008). SANISAND: Simple anisotropic sand plasticity model. *Int. J. Numer. Analyt. Meth. Geomech.*, **32**, No. 8, 915-948. **doi**: 10.1002/nag.651.

Woo, S. I. & Salgado, R. (2015). Bounding surface modeling of sand with consideration of fabric and its evolution during monotonic shearing. *Int. J. Solids Struct.,* **63**, 277-288. **doi**: 10.1016/j.ijsolstr.2015.03.005.

Wood, D. M., Diambra, A. & Ibraim, E. (2016). Fibres and soils: a route towards modelling of root-soil systems. *Soils Found.,* **56**, No., 5, 765-778, **doi**: 10.1016/j.sandf.2016.08.003.

Zornberg, J. (2002). Discrete framework for equilibrium analysis of fibre reinforced soil. *Géotechnique*, **52**, No. 8, 593-604, **doi**: 10.1680/geot.2002.52.8.593.